MODELING BIMODAL WIND-WAVE PROPAGATION RESONANCE

W. Erick Rogers, Paul A. Hwang, James M. Kaihatu, and David W. Wang

Oceanography Division, Naval Research Laboratory, Stennis Space Center, MS, USA

1. INTRODUCTION

A high-resolution, airborne topographic mapper was deployed in the Gulf of Mexico on November 5, 1998 during a period of fetch-limited wave conditions (winds directed offshore). A cross-hatched pattern is observed in the free surface disturbances associated with the local sea. In the very nearshore, the wave fronts indicate that wave propagation is almost normal to the wind direction. As fetch increases, waves grow longer and higher, and the wave directions steer to be closer to that of the wind (free surface topography and associated directional spectra are show in Fig. 1). We hypothesize that this is a demonstration of the propagation resonance phenomenon described by Phillips (1957). The propagation resonance condition given by Phillips is satisfied by two solutions:

$$\theta_r = \pm \cos^{-1}(C_p / U_r), \qquad (1)$$

where θ_r is the angle between the wind direction and the wave direction, C_p is the wave phase velocity, and U_r is the wind speed at a reference height proportional to the wavelength (we use $U_r \equiv U_{1/k}$, where k is the component wavenumber). In this study, we attempt to recreate what we observe in the data using a third generation wave model. This type of model is phase-averaged, so processes such as wind input, nonlinear interactions, and wave breaking are represented by energy source/sink terms. The wind input formulations presently used by such models are unimodal, with a peak at θ=0. We replace the unimodal source term with a bimodal source term, with peaks described by (1). It is hoped that further development of this modified source term will allow a more accurate representation of early-stage and short-fetch wave growth by wave models.

2. DATA SET

In data set studied here, the wind was from 310-350° (NNW), with U_{10} of 9.4-10.8 m/s during the four hours prior to the airborne measurement. A light southerly swell is also seen in the topographic data; it is easily distinguished from the fetch-limited local seas. Data was taken along a transect corresponding to a fetch of 0-42km. The lidar data collection system is described in detail in Hwang et al. (2000a,b), and its deployment for this data set is described further in Hwang et al. (2000c).

2.1 Discussion: "Ground Truth"

Though a wave model can often predict wave height and peak frequency with adequate skill, predictions of directional distributions are of more dubious accuracy. To a large extent, this can be blamed on the lack of adequate directional data. Directional data typically come in the form of truncated Fourier series. This information can be very useful to a wave modeler, but some assumptions must be made to convert to actual directional spectra. Thus, these spectra cannot, strictly speaking, be used as ground truth for a model. Free surface topographic data, on the other hand, does provide a ground truth, and therefore provides a useful tool for evaluating or developing the directional capabilities of a numerical model.

3. THE WAVE MODEL

We use the third generation wave model SWAN ("Simulating WAves Nearshore", Booij et al. 1999). It is governed by a form of the two-dimensional hyperbolic wave equation, expressed in terms of the wave action density spectrum:

$$N(x, y, \sigma, \theta) = \frac{E(x, y, \sigma, \theta)}{\sigma}, \qquad (2)$$

where N is wave action density, E is wave energy density, x and y denote geographic location, σ is the relative frequency, and θ is the direction of propagation. Wave action is propagated in geographic and spectral space, while source and sink terms act on the waves. The action balance equation, in horizontal Cartesian coordinates (x,y), can be written as

$$\frac{\partial}{\partial t} N + \frac{\partial}{\partial x} C_{gx} N + \frac{\partial}{\partial y} C_{gy} N + \frac{\partial}{\partial \sigma} C_\sigma N + \frac{\partial}{\partial \theta} C_\theta N = \frac{S}{\sigma}. \qquad (3)$$

(e.g., Whitham 1974; Phillips 1977; Mei 1983; Hasselmann et al. 1973). Here, t denotes time, C_g is group velocity, C_σ is wave action propagation speed in σ-space, C_θ is propagation speed in θ-space, and S

denotes the total of source and sink terms. The first term represents the local rate of change; the second and third terms represent geographic propagation; the fourth term represents changes to relative frequency (e.g. by nonstationary depth or by currents); the fifth term represents refraction (by depth and currents).

The primary components of S in deep water are

$$S = S_{in} + S_{ds} + S_{nl}, \quad (4)$$

where S_{in} represents input by wind (described below), S_{ds} represents steepness-limited breaking (a tuned closure term, see Komen et al. 1984), and S_{nl} is the model's approximation of four-wave interactions (DIA, Hasselmann et al. 1985). S_{in} has two components:

$$S_{in}(\sigma,\theta) = A + BE(\sigma,\theta). \quad (5)$$

The term A represents linear growth (e.g. Phillips 1957; Cavaleri and Malonotte-Rizzoli 1981; Tolman 1992; Ris 1997):

$$A = \frac{1.5\times10^{-3}}{g^2 2\pi}\left[U_* \max[0,\cos(\theta_d)]\right]^4 F \ , \quad (6)$$

$$F = \exp(-(\sigma/\sigma^*_{PM})^{-4}), \quad (7)$$

$$\sigma^*_{PM} = \frac{0.13g}{28U_*}2\pi, \quad (8)$$

where g is gravity, U_* is the friction velocity, F is a filter, and σ_{PM} is the equilibrium peak frequency for a fully-developed sea state (Pierson and Moskowitz 1964), i.e., duration- and fetch-unlimited conditions.

The term B represents exponential growth (e.g. Miles 1957; Snyder et al. 1981; Komen et al. 1984):

$$B = \max\left[0, 0.25\frac{\rho_a}{\rho_w}\left[28\frac{U_*}{C}\cos(\theta_{wv}-\theta_{wd})-1\right]\right]\sigma, \quad (9)$$

where ρ_a and ρ_w are the densities of air and water, and θ_{wv} and θ_{wd} are the directions of the wave component and the wind, respectively.

The values of the free parameters of the breaking term are based on the work of Komen et al. (1984), who used two free parameters to tune the model to match the Pierson and Moskowitz (1964) values for fully-developed conditions. No such tuning has been conducted to match data under fetch-limited conditions; however, SWAN has been compared by Ris (1997) to data and empirical expressions for dimensionless wave energy and peak frequency, and the model is shown to be reasonably accurate.

4. PROPAGATION RESONANCE

Our aim in this paper is to answer the question: "can the development of bimodal directional distribution observed in this data set of 3D surface wave topography be reproduced by incorporating the Phillips propagation resonance (as shown in (1)) into a third generation wind-wave model?". Thus we do not (yet) concern ourselves with issues such as accuracy of model forcing (winds) or tuning the modified model for general usage. With a more thorough data set, it may be possible to a) verify that this bimodality is a consistent feature of a young wave field, b) verify that it is, indeed associated with the resonance mechanism of (1), and c) tune the model such that proper development of directional spectra is achieved under a variety of conditions.

4.1 Kinematics

The kinematics of (1) are quite simple: the crests of a wave will align such that the speed of the crest, measured along the axis of the wind, is identical to the velocity of the wind (at some physically meaningful, reference height). In a phase-average sense, this steering, or realignment, occurs as wave energy satisfying the resonance condition is enhanced, while wave energy not satisfying the condition is diminished (one can expect non-forced short waves to be quickly attenuated).

4.2 Implementation

As a practical matter (for wave modeling purposes) we must allow some energy be transmitted to wave energy with directions slightly different from the resonance-preferred direction(s). We use the $\max(0,\cos^n(\theta))$ form traditional in wave modeling, with n=1, as used in the Snyder et al. (1981) wind input term (9)1. Thus a modified form of B, replacing θ_{wd} with $\theta_{wd}\pm\theta_r$, would be

$$B = \max\left[0, 0.25\frac{\rho_a}{\rho_w}\left[28\beta\frac{U_*}{C}\cos(\theta_{wv}-(\theta_{wd}+\theta_r))-1\right]\right]\sigma$$

1 Note added Oct. 2002: We had two choices
1) Only make the linear growth term bimodal; this is the term that is related to Phillips resonance theory, but is far too weak to give the kind of growth that we see in the data, or
2) Use the exponential growth term, which is close to the correct magnitude seen in data (within a factor of 2, say), but is based on theory unrelated to Phillips resonance theory.
We chose (2).

$$+\max\left[0,0.25\frac{\rho_a}{\rho_w}\left[28\beta\frac{U_*}{C}\cos(\theta_{wv}-(\theta_{wd}-\theta_r))-1\right]\right]\sigma \quad (10)$$

Here, β is an empirical factor. Komen et al. (1984)) discuss this factor, and use a value of 1.0, noting that it has little effect on results (at least for fully-developed conditions). In order that total stress is consistent with that of the Komen et al. formula, β should be taken as $\beta = 1/\sqrt{2}$. However, the actual value of β is not important for our purposes, as the actual values of U_* which we use are somewhat arbitrary. We note that β would need to be considered in any subsequent tuning exercise.

We make the linear growth term A bimodal in a manner similar to (10).

4.3 Model input

For model input, we assume deep water, with constant and uniform wind forcing (a reasonable assumption for fetch-limited growth of this scale). Herein, we present results from three simulations of the model with the bimodal source term, using U_{10}=8.5, 10, and 12 m/s, with β=1.0. The simulations are duration-unlimited (steady state).

Though there is a mild swell system apparent in the data, we do not include the swell as boundary forcing, for the simple reason that sea-swell interaction is not represented in the model in a physically meaningful way. To give an example, the dissipation formulation of SWAN, based on WAM cycle 3, is a function of the average steepness of the entire wave spectrum. Thus, whitecapping is reduced by the presence of swell (which is generally not steep). Though it may be argued that swell can indirectly reduce breaking via reduction of roughness and therefore wind input, this is not how the model is formulated. The effect of swell on wind sea growth in the model requires further refinement, so inclusion of swell in the simulation is undesirable if we are interested only in the wind sea portion of the spectrum.

4.4 Model results

Table 1 shows results at a point corresponding to a fetch of about 38km for the original and modified source terms, and compares to data. It is clear from this that, with the original model, there is significant error in the predicted non-directional parameters (T_{peak} and H_{m0}). Thus, a modified model can either match the data, or the original model (not both). To recover the T_{peak} result of the original model, a lower wind speed is needed (8.5m/s). This is expected, as β=1.0 is used in the modified model (and not $\beta = 1/\sqrt{2}$). Figs. 2a, b show the evolution of the directional spectra with fetch for two modified models for comparison to Fig. 1b (U_{10}=10, and 12 m/s). The U_{10}=12 m/s simulation does a reasonably good job of capturing, at least qualitatively, the spectral evolution seen in the data. The spreading of the frequency spectra seems to be underpredicted by the model, while the directional spreading of the lobes is overpredicted. The former is probably (primarily) a direct result of the simplified wind forcing. The latter indicates that a narrower source term might be more accurate, e.g. S_{in}=f(max(0,cos^2(θ))) rather than S_{in}=f(max(0,cos(θ))).

Table 1. Comparison of wave parameters at 38km fetch

Source	T_{peak} (sec)	H_{m0} (m)	θ_{peak} (degrees from primary wind direction)
Lidar data	4.5-5.2	0.9	-80, +50
Original model, U_{10}=10m/s	4.1	1.1	0
Modified model, U_{10}=8.5m/s	4.1	1.2	±25*
Modified model, U_{10}=10m/s	4.3	1.3	±40*
Modified model, U_{10}=12m/s	4.4	1.5	±55

* : the two modes are merged, so the result is unimodal in appearance.

5. DISCUSSION

5.1 Unrepresented Processes

The bimodality observed in the data suggests two possibilities. Either

a) the wave energy is generated, centered at $\theta_{wv}=\theta_{wd}$ (as a traditional wave model would predict) and quickly steered/transferred to the oblique modes, or
b) the transfer of energy from the wind to the wave system (i.e. the wind input S_{in}) is itself bimodal.

We feel that the latter is the case, and further that the resonance mechanism described by (1) is responsible for the bimodality of dominant waves. Whatever the case may be, it can be said with some certainty that the responsible mechanism is not represented in existing wave models. The traditional mechanism for creating bimodal wave patterns in a wave model is four-wave interactions, S_{nl}. However, this mechanism does not create bimodality near the spectral peak, as seen in the data, but rather, at the higher and lower ends of the frequency spectrum. Thus this mechanism is tentatively ruled out for explaining the observed bimodal propagation of dominant waves.

There are other processes which, though unlikely to be responsible for the bimodality of the observed spectra, do deserve attention. This is especially true since certain aspects of the data cannot be explained by the resonance mechanism: 1) the waves stay at a cross-wind direction for a longer fetch than would be predicted by the Phillips resonance, and 2) the directional modes of the data are asymmetric with respect to the wind direction. The underlying current field, neglected here, may be important: typically, though most wave models are designed to account for the effects of currents on waves, currents are not included in model forcing, simply because no reliable (and/or adequately resolved) surface current information exists (as in this case). Another issue is the possible hydrodynamic modulation of wind sea by swell, which though perhaps significant, is not faithfully represented in the model. The underlying currents and/or swells is thought to be a likely cause of the asymmetry of the data, since the effect of currents/swell on wind sea is, of course, directionally dependent.

5.2 Fetch-limited Growth Curves

The implementation of the resonance mechanism of (1) in a wave model would have a significant impact on fetch-limited growth curves predicted by the model. Existing models are reasonably effective at matching the Kahma and Calkoen (1992) curve for moderate fetches. Ideally, a modified model, after tuning, would produce, more or less, the same result for such fetches. However, one can expect predictions for shorter fetches to be quite different. Perhaps the most obvious difference would be at the model origin (zero fetch). A traditional model will always predict zero energy at this origin, while the modified model will have energy there, due to waves traveling almost normal to the wind direction and even (due to the cosine distribution of the source term) waves traveling obliquely against the wind direction.

6. SUMMARY

Free surface topography was acquired for a fetch-limited wind growth case in the Gulf of Mexico on Nov. 5, 1998, from which ground truth directional spectra were derived along the fetch axis. In these directional spectra, we observe two directional modes, both oblique to the wind direction (Fig. 1). In this paper we have demonstrated that it is possible to qualitatively recreate this result in a third generation wave model by replacing the unimodal source term with a bimodal source term, with the two peaks being described by the solutions for Phillips propagation resonance, (1). Some unresolved issues remain; the most notable listed here:

1) We believe that this resonance mechanism is the most likely cause of the bimodality of dominant waves and demonstrate how it is possible. However, we do not prove conclusively that this is, in fact, the cause.
2) Frequency distributions predicted by the model are much narrower than that of the data.
3) Directional distributions of the two modes predicted by the model are broader than the data.
4) The two modes in the data are slightly asymmetrical; the cause of this is not clear, though interaction of the wind sea with swell and/or currents is a suspected cause.
5) Any implementation of this mechanism in an operational model would necessitate significant retuning of the model source term(s).

ACKNOWLEDGEMENT

This work is supported by the Office of Naval Research (Naval Research Laboratory Program Element N62435, “Phase Resolved Nonlinear Transformation of Shoaling Waves.”, NRL Contribution PP/7320-00-1010).

REFERENCES

Booij, N., R. C. Ris, and L. H. Holthuijsen, 1999: A third-generation wave model for coastal regions, 1, Model description and validation. *J. Geophys. Res.*, **104**, 7649-7666.

Cavaleri, L. and P. Malonotte-Rizzoli, 1981: Wind wave prediction in shallow water: theory and applications. *J. Geophys. Res.*,**86**, No. C11, 10961-10973.

Hasselmann, K., and Coauthors, 1973: Measurements of wind-wave growth and swell decay during the Joint North Sea Wave Project (JONSWAP). *Dtsch. Hydrogr. Z.*, Suppl., **12**, A8.

Hasselmann, S., K. Hasselmann, J. H. Allender, and T. P. Barnett, 1985: Computations and parameterizations of the linear energy transfer in a gravity wave spectrum, II, Parameterizations of the nonlinear transfer for application in wave models. *J. Phys. Oceanogr.*, **15**, 1378-1391.

Hwang, P. A., D. W. Wang, E. J. Walsh, W. B. Krabill, and R. N. Swift, 2000a: Airborne measurements of the wavenumber spectra of ocean surface waves. Part 1. Spectral slope and dimensionless spectral coefficient. *J. Phys. Oceanogr*. (in press).

Hwang, P. A., D. W. Wang, E. J. Walsh, W. B. Krabill, and R. N. Swift, 2000b: Airborne measurements of the wavenumber spectra of ocean surface waves. Part 2. Directional distribution. *J. Phys. Oceanogr*. (in press).

Hwang, P. A., D. W. Wang, W. E. Rogers, and J. M. Kaihatu, 2000c: A discussion on the directional distribution of wind-generated ocean waves. Proceedings, *6th International Workshop on Wave Hindcasting and Forecasting*, Monterey, California.

Kahma, K. K., and C. J. Calkoen, 1992: Reconciling the discrepancies in the observed growth of wind-generated waves. *J. Phys. Oceanogr.*, **22**, 1389-1405.

Komen, G. J., S. Hasselmann, and K. Hasselmann, 1984: On the existence of a fully developed wind-sea spectrum. *J. Phys. Oceanogr.*, **14**, 1271-1285.

Mei, C. C., 1983: *The applied dynamics of ocean surface waves,* Wiley, New York, 740pp.

Miles, J. W., 1957: on the generation of surface waves by shear flows, *J. Fluid Mech.*, **3**, 185-204.

Phillips, O. M., 1957: On the generation of waves by turbulent wind. *J. Fluid Mechanics*, **2**, 417-445.

Phillips, O. M. 1977: *The dynamics of the upper ocean, 2nd edition*, Cambridge University Press, 336pp.

Pierson, W. J., and L. Moskowitz, 1964: A proposed spectral form for fully developed wind seas based on the similarity theory of S. A. Kitaigorodsii. *J. Geophys. Res.*, **69(24)**, 5181-5190.

Ris, R. C., 1997: *Spectral modeling of wind waves in coastal areas.* Ph.D. thesis, Delft University of Technology, 160pp.

Snyder, R. L., F. W. Dobson, J. A. Elliot, and R. B. Long, 1981: Array measurement of atmospheric pressure fluctuations above surface gravity waves. *J. Fluid Mech.* **102**, 1-59.

Tolman, H. J., 1992: Effects of numerics on the physics in a third-generation wind-wave model, *J. Phys. Oceanogr.*, **22**, No. 10, 1095-1111.

Whitham, G. B., 1974: *Linear and nonlinear waves,* Whiley, New York, 636pp.

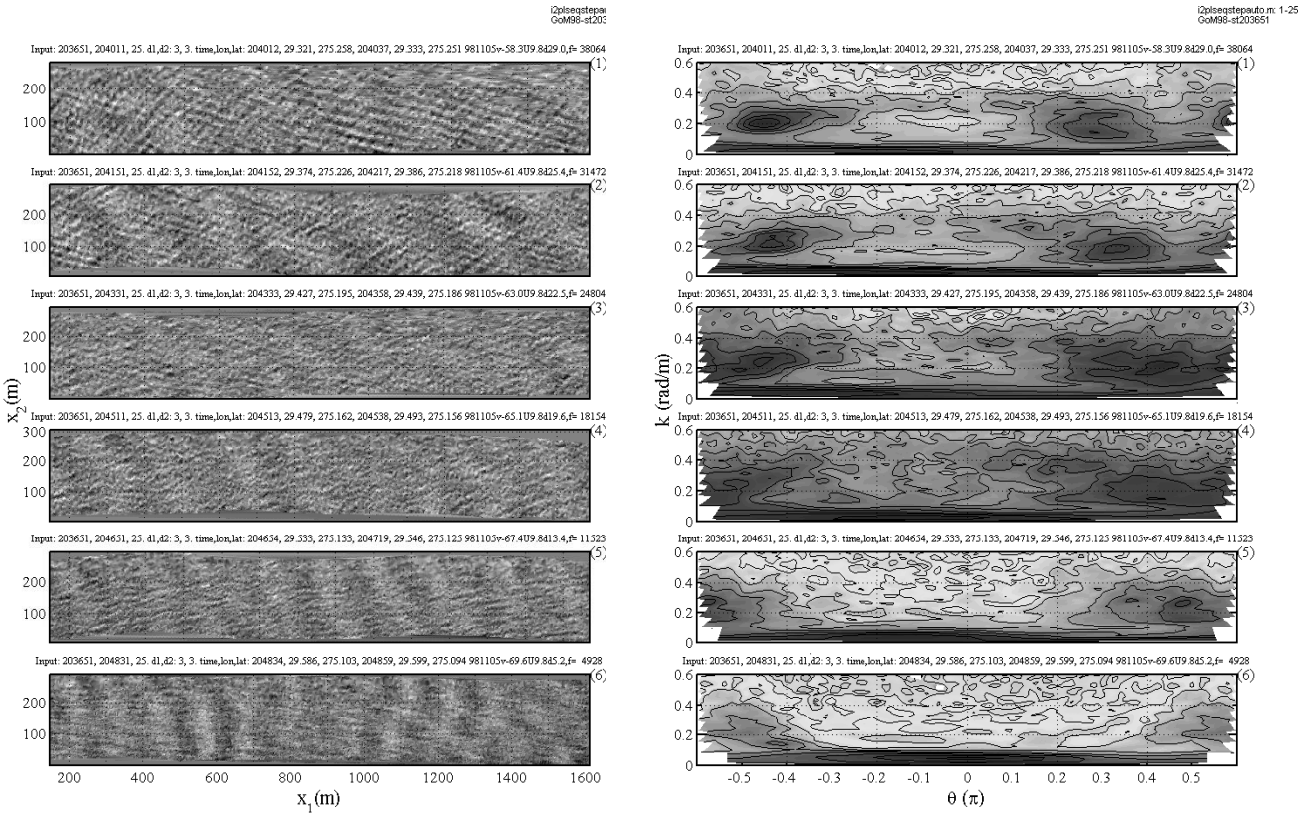

Figure 1. Left diagram: Surface wave topography at six different fetches. Wind is from right to left (offshore fetch growth condition). Right diagram: The corresponding directional spectra. The wind direction is at θ=0. The fetches for the six cases are 38.1, 31.5, 24.8, 18.2, 11.5 and 4.9 km from top to bottom [Hwang et al. 2000c].

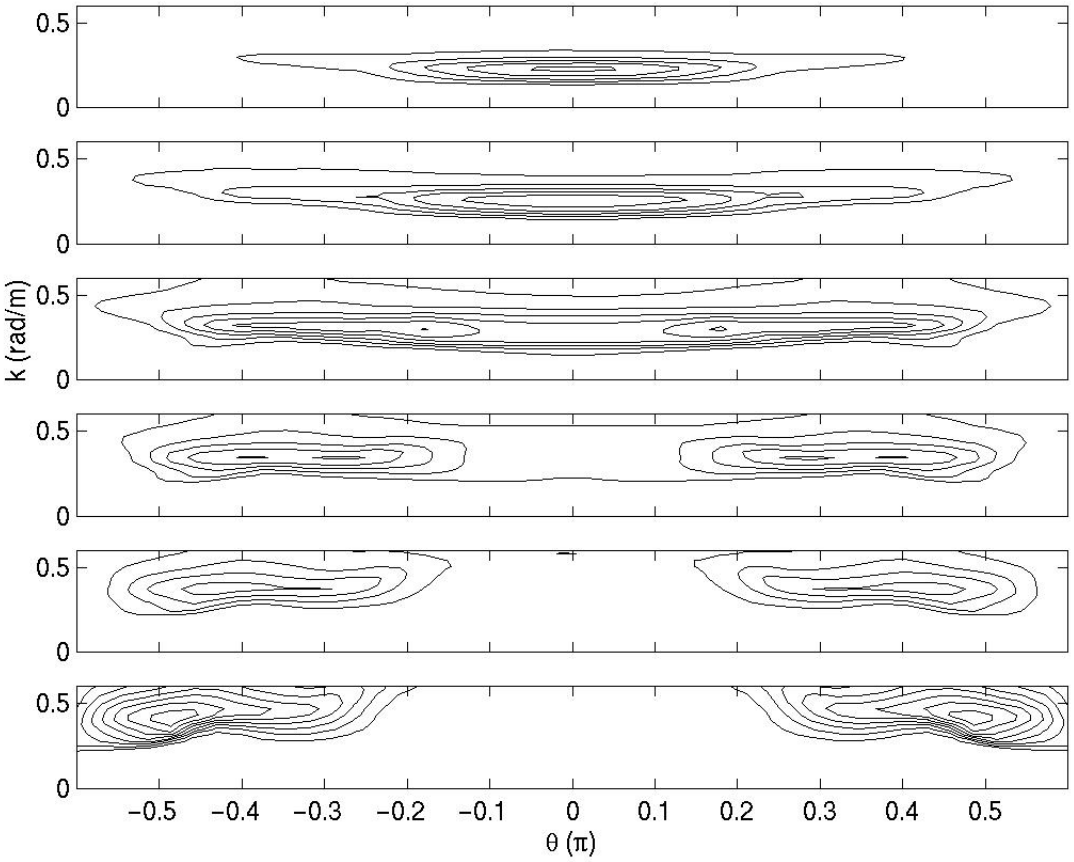

Figure 2a. Directional spectra $S(f,\theta)$ at six locations, corresponding to the locations of lidar measurements in Fig. 1. From top to bottom, fetch is 38.1, 31.5, 24.8, 18.2, 11.5, and 4.9 km. U_{10}=10 m/s.

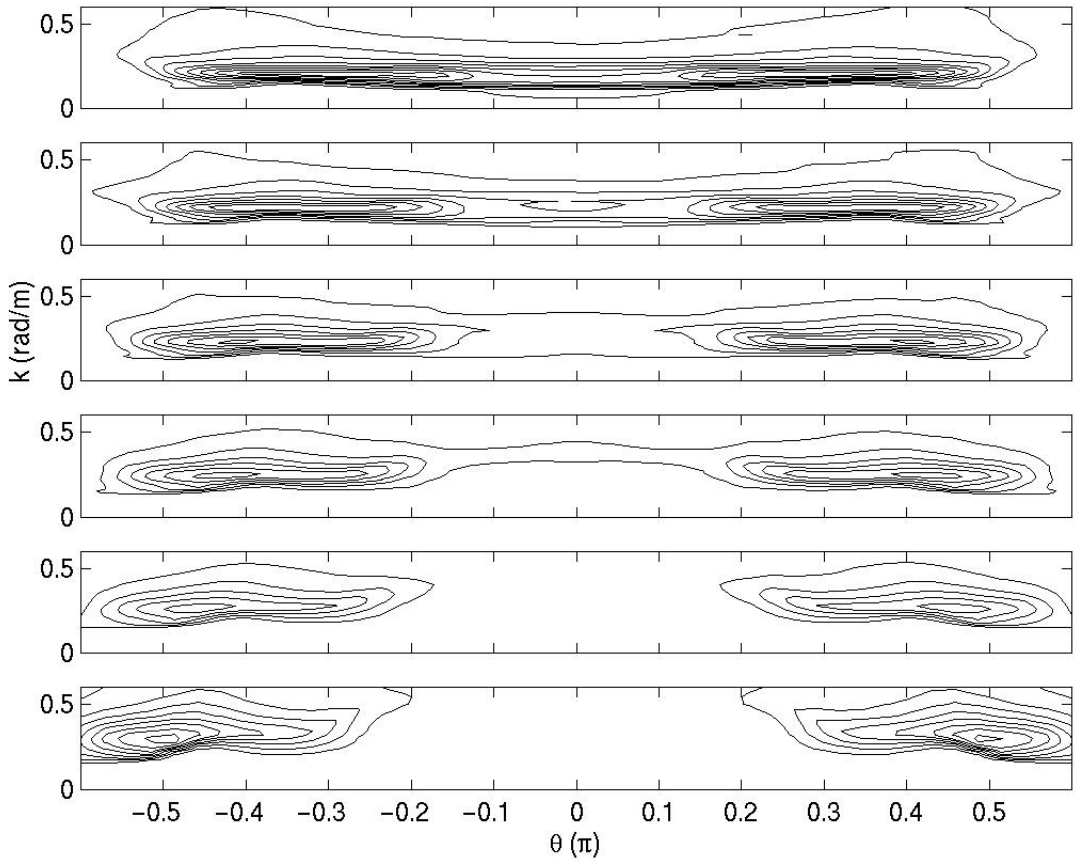

Figure 2b. Directional spectra $S(f,\theta)$ at six locations, corresponding to the locations of lidar measurements in Fig. 1. From top to bottom, fetch is 38.1, 31.5, 24.8, 18.2, 11.5, and 4.9 km. U_{10}=12 m/s.